Journal of Power Sources 217 (2012) 102–107

Contents lists available at SciVerse ScienceDirect

Journal of Power Sources

journal homepage: www.elsevier.com/locate/jpowsour

Si–Y multi-layer thin films as anode materials of high-capacity lithium-ion batteries

Haixia Li, Hongmei Bai, Zhanliang Tao*, Jun Chen

Key Laboratory of Advanced Energy Materials Chemistry (Ministry of Education), College of Chemistry, Nankai University, No. 94 Weijin Road, Tianjin 300071, People's Republic of China

HIGHLIGHTS

- ► Si–Y multi-layer thin films have been prepared by radio frequency magnetron sputtering.
- ► The sample with the Y thin film of 22.5 nm shows excellent cycle performance.
- ► The Y thin film can act as a buffer layer to improve the Li-ion kinetic property.

ARTICLE INFO

Article history:
Received 21 March 2012
Received in revised form
9 May 2012
Accepted 28 May 2012
Available online 5 June 2012

Keywords:
Lithium-ion battery
Anode material
Multi-layer thin films
Magnetron sputtering

ABSTRACT

In this paper, we report on the preparation of Si–Y multi-layer thin films by magnetron sputtering and their application as anode materials of lithium-ion batteries. Scanning electron microscopy (SEM) with energy dispersive X-ray (EDX) and transmission electron microscopy (TEM) have been used to characterize the morphologies and structures of the as-prepared thin films. The framework of the Si–Y thin films is Y-Si-Y-Si multi-layers, including the Si thin film with a thickness of 225 nm and the Y thin film with different thickness (15–37.5 nm). The electrochemical performance of the samples is investigated by charge–discharge measurement, cyclic voltammetry and electrochemical impedance spectra (EIS). Compared with pure Si thin film, the Si–Y thin films with the optimal Y film thickness of about 22.5 nm can deliver a high reversible capacity of 2450 mAh g^{-1} under a current density of 0.4 C after 50 cycles, showing superior cycle performance and electrode stability due to the better Li^+ diffusion character. This study should shed light on the design and application of Si–Y multi-layer thin films as anode materials of high-capacity lithium-ion batteries.

1. Introduction

Thin-film lithium-ion batteries are promising candidates for micro-power sources due to small size, long cycle-life, high energy density and reliability [1–4]. Recently, a great deal of attention has been focused on the research and development of thin film materials with different methods for the application of thin-film lithium-ion battery [5,6]. For example, lithium alloys especially Li with C, Sn, Si and other metals have been studied as thin-film anode materials [7–12]. Among them, Si is one of the most promising materials with a suitably low potential for lithium intercalation and a high theoretical specific capacity (4200 mAh g^{-1}, $Li_{22}Si_5$) [13–15]. Unfortunately, substantial volume changes of Si thin film cause fast cracking and pulverization of the electrode, resulting in rapid capacity fading [16–18].

Researchers have made attempts to improve the electrochemical performance of Si thin film as anode material, among which the introduction of a secondary material is an effective way [19–21]. The secondary material that can be either electrochemically active or inactive toward lithium has shown to some extent in a number of systems such as Si–M (M = Ti, C, Sn) [22–24]. Similarly, the rare earth Y, which is inactive toward lithium, has been studied to combine with Al to form a hybrid composite as the anode material [25]. The secondary material Y is used to alleviate the volume change in the electrode and to prevent the aggregation of the active materials. Additionally, an effective way to implement the above-described concept is to use a multi-layer thin film comprising Si and metal layers (such as Ti, Al, Zn and Ge) in which the metal has a strong affinity toward Si [26–28]. In the multi-layer thin films, a stable structure of the metal–silicon interface may be allowed due to the strong bonding character between metal atoms

* Corresponding author. Tel.: +86 22 23506808; fax: +86 22 23509571.
E-mail address: taozhl@nankai.edu.cn (Z. Tao).

0378-7753/$ – see front matter © 2012 Elsevier B.V. All rights reserved.
http://dx.doi.org/10.1016/j.jpowsour.2012.05.080

and Si [29]. However, to the best of our knowledge, the study of Si–Y composite thin films as the anode of Li-ion batteries is still limited.

In this article, we report the preparation of Si–Y multi-layer thin films on copper foam substrate by radio frequency (RF) magnetron sputtering and their application as the anode material of lithium-ion batteries. The effect of the thin-film thickness on the electrochemical performance has been studied. It is found that Y sub-thin film can act as a buffer layer to reduce the effect of the volume expansion during charge–discharge cycling test. The present results show that Si–Y multi-layer thin films have potential as the anode materials of high-capacity lithium-ion batteries.

2. Experimental

2.1. Electrode preparation

The Si–Y thin films were prepared layer-by-layer (Y-Si-Y-Si) in a JCP-350 multi-target magnetron sputtering system with the n-type monocrystalline Si (99.99%) and Y (99.99%) as the targets and copper foam as the substrate. The base pressure was 5.0×10^{-4} Pa. The high-purity argon (99.999%) was introduced into the stainless-steel chamber before sputtering. The working pressure was kept at 0.50 Pa controlled by an argon flow rate of 20.0 sccm [30]. The substrate temperature was controlled at 300 °C, and the rotating speed of the substrate was 15 r min^{-1}. Si–Y multi-layer thin films were deposited on both the glass for microstructure characterization and the copper foam for electrochemical test. Before the deposition on the substrate, the targets were pre-sputtered for 10 min to remove the contaminants on the surface. For the first step, Y thin film was deposited onto the substrate, and then followed by the deposition of Si thin film. The above two-step experiment was repeated to obtain the Si–Y multi-layer thin films. The Si layers were deposited using a constant power density of 5.1 W cm^{-2} on the Si target with a deposition rate of 5 nm min^{-1}. The deposition times for Y target were varied to create layers of different thickness with a deposition rate of 15 nm min^{-1} at a power density of 0.82 W cm^{-2}. The Si thin film was deposited in 45 min, and the Y thin film was obtained by sputtering for 60 s, 90 s, 120 s and 150 s. For comparison, the pure Si thin film was prepared under the same conditions. The amount of the deposited thin films was measured by electronic analytical balance (Sartorius-BS224S, resolution of 0.1 mg) in combination with electronic quasi-microbalance (Sartorius-BT25S, resolution of 0.01 mg).

2.2. Characterization

The morphologies and thickness of the thin films were characterized by scanning electron microscopy (SEM, FEI NanoSEM 430). The composition and structure of the films were analyzed by an energy dispersive X-ray (EDX) analyzer attached to the SEM. Crystallinity and the layered structure of the as-prepared samples were investigated by transmission electron microscopy (TEM, Philips Tecnai F20, 200 kV) [31].

2.3. Electrochemical measurement

The 2032 button cells were assembled to take the electrochemical measurement [32]. High-purity metallic lithium was used as the counter electrode with the reference electrode, and the working electrode was the Si–Y thin film deposited on copper foam. The cell was assembled in a glove box (Mikrouna China Universal 2240/750). The electrolyte comprises 1 mol L^{-1} $LiPF_6$ in a 1:1 (volume ratio) mixture of ethylene carbonate (EC) and diethyl carbonate (DEC) [33]. Cyclic voltammetry measurements and charge/discharge tests were carried out on the electrochemical workstation (Potentiostat/Galvanostat Model 263A) and the Land battery test system (Land, CT2001A), respectively. Cyclic voltammetry (CV) was conducted between 0.01 and 2.0 V versus Li/Li^+ at various scan rates from 0.10 to 0.25 mV s^{-1}. For charge–discharge tests, all cells were tested under a current density of 0.4 C up to 50 cycles. Electrochemical impedance spectroscopy (EIS) measurements were carried out on a Parstat 2273 potentiostat/galvanostat analyzer (Princeton Applied Research & AMETEK Company). When the electrode was charged up to 2.0 V versus Li^+/Li, it was left on open-circuit for 2 h to obtain the equilibrium state at 25 °C, and then EIS was measured over the frequency range from 6×10^4 to 1×10^{-2} Hz with AC amplitude of 5 mV. ZsimpWin software was used to analyze the EIS results [34].

3. Results and discussion

3.1. Characterization

By changing the sputtering time of the yttrium target, we have prepared the Si–Y multi-layer thin films with different thickness. In comparison, we obtain the thickness from the characterization of the cross-section of the samples deposited on the glass. Table 1 summarizes the parameters of Si–Y multi-layer thin films grown by the magnetron sputtering.

Fig. 1 shows the SEM and TEM images with EDX analyses of sample with the thickness of Y thin film of 22.5 nm. Fig. 1a shows the SEM image of the sample, displaying the three-dimensional structure of copper foam that is covered with Si–Y thin film. The as-prepared materials are observed to have a dense structure, which can be seen from the amplified image in Fig. 1b. The Si–Y multi-layer thin film shows a rough surface because the surface profile of the copper foam is reflected in the morphology of Si–Y thin film. The EDX image in Fig. 1b confirms the presence of silicon and yttrium. The TEM image of the sample in Fig. 1c reveals that two elements are of alternative distribution. The dark areas are Y element and the light areas are Si element. From the HRTEM image in Fig. 1d, we can clearly see the lattice fringes of Y but no lattice line in the image of Si. The image got from Fourier transformation is well indexed as a pure hexagonal Y phase. This proves that Y is crystalline and Si is amorphous. As known, Si and Y can form alloy such as YSi_2 in the phase diagram [35]. However, the substrate temperature (300 °C) during the experiment is far below the formation temperature of Si–Y alloys (>1200 °C) in the phase diagram. Furthermore, there are no lattice fringes to show the binary alloy phase from the HRTEM. The above information proves that there is no chemical reaction between Si and Y. To more clearly demonstrate this multi-layer structure, we prepared the thick Si–Y thin film on the glass and made the cross-section of the sample to construct the EDX mapping (Fig. 1e–g). The Si and Y elements are expressed as red and green, respectively. The result can evidently illustrate the layered architecture of the sample. The other three

Table 1
Parameters for the preparation of Si–Y multi-layer thin films.

System	Sputtering time		Monolayer thickness (nm)		multi-layer thickness (nm)
Si–Y multi-layer	Si (min)	Y (s)	Si	Y	
Y-Si-Y-Si	45	60	225	15	480
		90		22.5	495
		120		30	510
		150		37.5	525

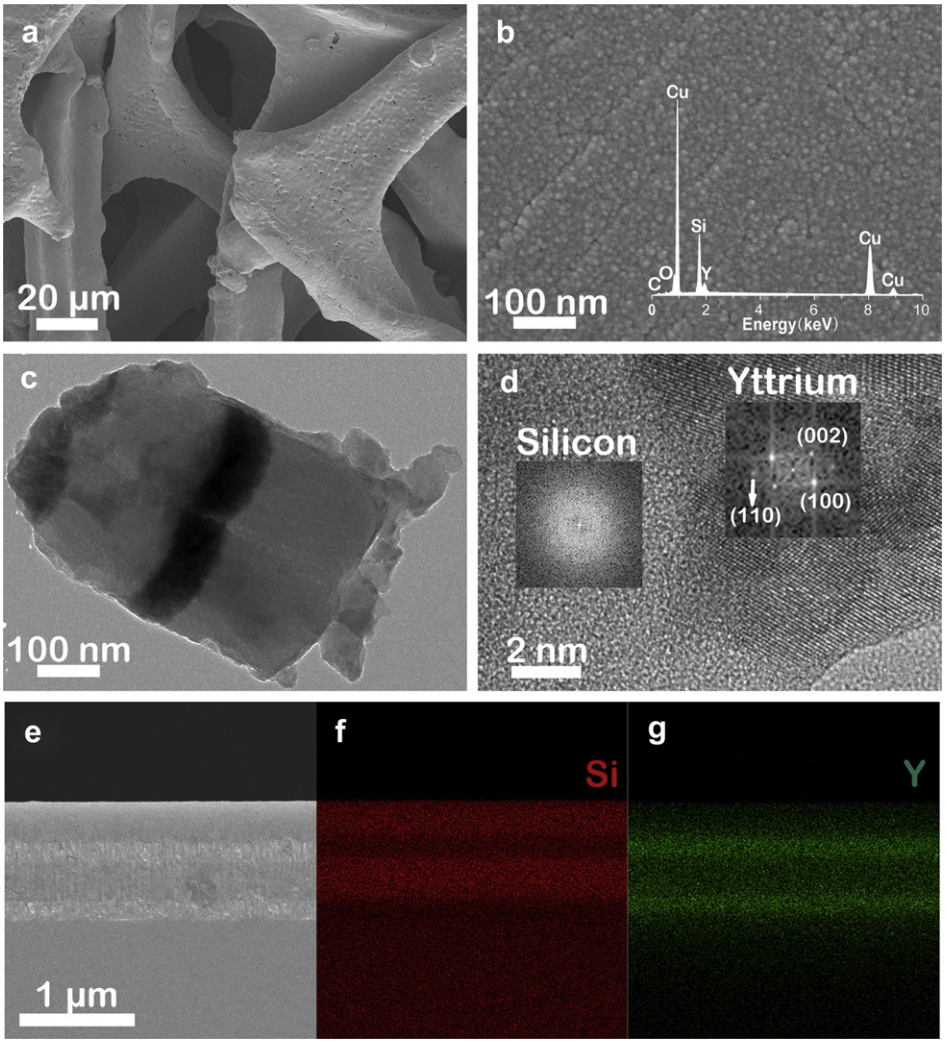

Fig. 1. (a, b) SEM image of Si–Y thin film deposited on copper foam of the sample with the thickness of Y thin film of 22.5 nm with the EDX analysis in the inset of (b). (c) TEM and (d) HRTEM image of Si–Y thin film scraped from the glass. (e–g) EDX mapping images of the cross section of Si–Y thin films deposited on the glass.

samples have the same character, but the multi-layer thickness is different.

3.2. Electrochemical measurements

Fig. 2 shows the cycling performance of pure Si and Si–Y multi-layer thin films with different thickness and the columbic efficiency

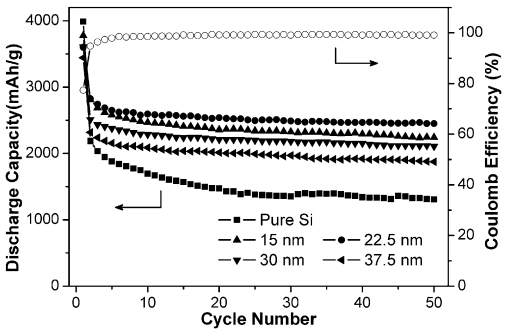

Fig. 2. Discharge capacity as a function of cycle number for pure Si thin film and Si–Y thin films with the thickness of Y thin film of 15, 22.5, 30, and 37.5 nm, and the columbic efficiency of the sample with the thickness of Y thin film of 22.5 nm.

of sample with the Y thin film of 22.5 nm. The charge–discharge capacities are normalized by the weight of composite thin film with Si and Y layers. The pure Si thin film shows an initial discharge capacity of about 3988 mAh g^{-1}, while the Si–Y multi-layer thin films deliver lower initial discharge capacities that are 3777, 3600, 3587 and 3441 mAh g^{-1} for the samples with the thickness of Y thin film of 15, 22.5, 30, and 37.5 nm, respectively. This means that the introduction of Y is inactive for electrochemical Li intercalation. However, the cycling ability of Si–Y anode is greatly improved in comparison with pure Si thin film. For pure Si, the capacity decreased sharply with the cycle number, reaching a value of 1306 mAh g^{-1} after 50 cycles that is 33% of the initial capacity. For the sample with the thickness of Y thin film of 37.5 nm that is slightly inferior in the four samples with Y addition, the capacity fading is still slower than that of pure Si. For the samples with the thickness of Y thin film of 30 and 15 nm, the capacities remained after 50 cycles are 2107 and 2242 mAh g^{-1}, respectively. Among the four samples, the sample with the thickness of Y thin film of 22.5 nm provides the highest capacity of 2450 mAh g^{-1} after 50 cycles that is 69% of the initial capacity. In the first cycle, the columbic efficiency of the sample with the thickness of Y thin film of 22.5 nm is 78%. The irreversible capacity is mainly attributed to the formation of a solid electrolyte interphase (SEI) layer in the first cycle. Furthermore, the columbic efficiency of the sample with the

thickness of Y thin film of 22.5 nm increases to above 95% at the second cycle and maintains a stable value in the subsequent cycles, indicating high charge and discharge efficiency of the Si–Y multi-layer thin film. Therefore, the electrochemical properties of the Si–Y anode are greatly affected by the thickness of the Y thin film. The buffer effect is not very obvious with the thin thickness of Y thin film (15 nm). With the increasing of the thickness of Y thin film, the buffer effect enhances. However, if the electrochemically inactive layer is too thick (such as Y thickness > 100 nm), it prevents Li ions from inserting in the active-material layers in the multi-layer electrodes because of the electrochemical inactivity toward lithium [36]. Among the tested four samples, the sample with Y (22.5 nm)-Si (225 nm)-Y (22.5 nm)-Si (225 nm) multi-layer thin films shows a better cycling performance.

Fig. 3 shows the charge–discharge curves of the Si–Y multi-layer thin films at selected cycles. Apparently, the sample with the thickness of Y thin film of 22.5 nm exhibits the best electrochemical performance, and the sample with the thickness of Y thin film of 37.5 nm is the worst. The thickness of the Y layer has effect on the electrochemical performance. The charge–discharge curves of films are smooth and sloped, which are the typical voltage profile of Li extraction/insertion in the amorphous silicon [37]. The voltage plateau range during discharging and charging is 0.4–0.01 V and 0.2–0.7 V, respectively.

Because the sample with the thickness of Y thin film of 22.5 nm has the best electrochemical performance in the four samples, we use it for further measurement and research. Fig. 4 shows the influence of the charge–discharge current on the capacity retention of the sample with the thickness of Y thin film of 22.5 nm. With the enhanced constant current, the capacity decreases regularly, but the downward trend is gradually slowing. The reversible capacity decreases from 2450 mAh g^{-1} at the current density of 0.4 C to 1250 mAh g^{-1} at the current density of 8 C. When the current density returns to 0.4 C, the capacity can be recovered,

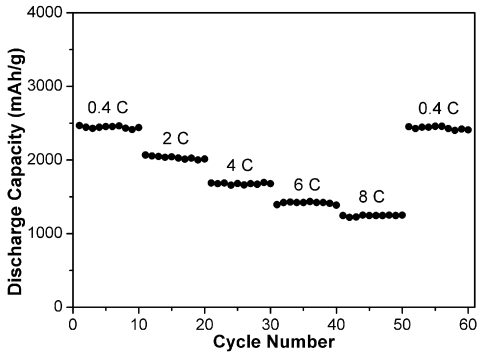

Fig. 4. Reversible discharge capacities of Si–Y thin film with the thickness of Y thin film of 22.5 nm at various charge–discharge current densities.

indicating that the sample has a good electrochemical reversibility and structural integrity.

To elucidate the reason for the improved Coulombic efficiency and stability of Si–Y anode, electrochemical impedance spectra (EIS) were implemented after charging the electrodes up to 2.0 V versus Li/Li^+. Fig. 5 shows the EIS graphs of Si and Si–Y thin films with the thickness of Y thin film of 22.5 nm after (a) 1st and (b) 30th cycle. The EIS plots are made up of only one depressed semicircle in high frequency and a following straight line in low frequency [38]. If the electrode is fully charged, the intrinsic electronic resistance and contact resistance of the electrode will be the principal factors that lead to the diameter of semicircle in high-frequency region [39]. Further, the high-frequency semicircle is related to the contact resistance of material and current collector [40]. The lost contact of material–material and material–current collector will give rise to the enlargement of high-frequency semicircle. In Fig. 5a, the Si–Y thin film demonstrates a lower high-frequency resistance than

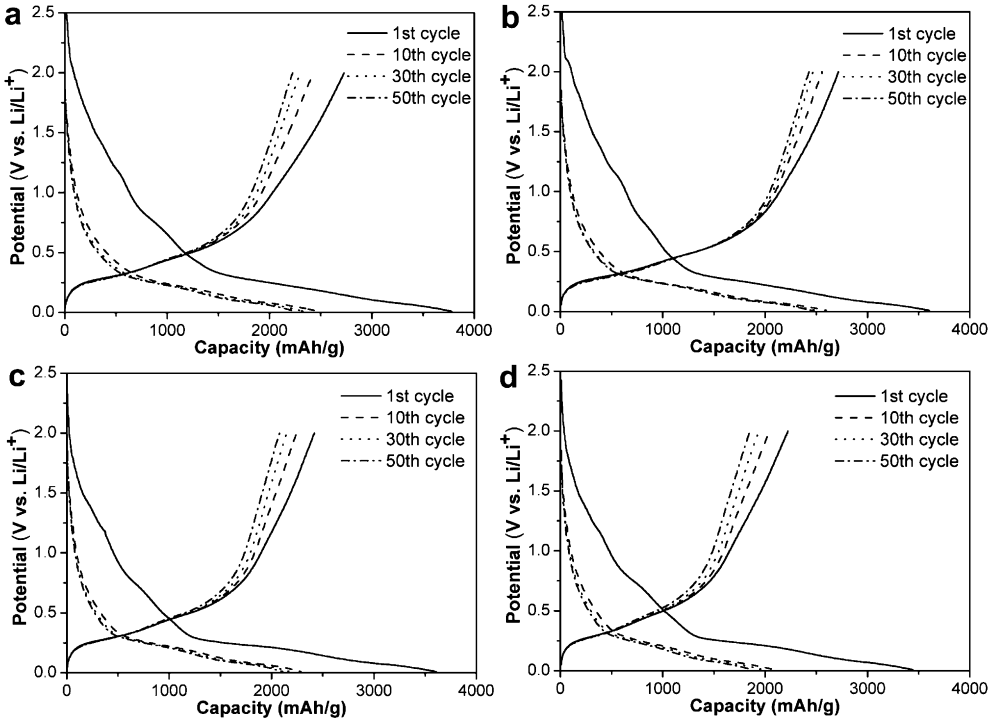

Fig. 3. Charge–discharge curves of Si–Y thin films with the thickness of Y thin film of (a) 15 nm, (b) 22.5 nm, (c) 30 nm, and (d) 37.5 nm under a current density of 0.4 C between 0.01 and 2.0 V versus Li/Li^+.

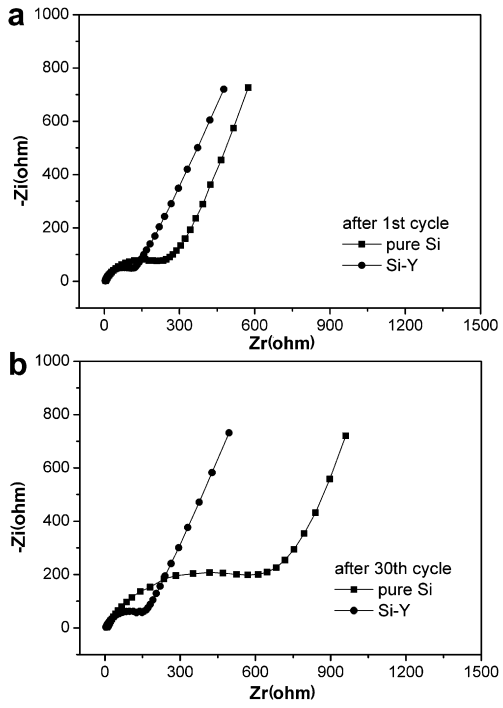

Fig. 5. EIS plot of pure Si thin film and Si–Y thin film with the thickness of Y thin film of 22.5 nm in the delithiated state after (a) 1st cycle and (b) 30th cycle.

pure Si after the first cycle. This indicates the smaller volume change of Si that is suppressed effectively by Y. Besides, Y as medium between Si and current collector can supply stronger adhesion between material and substrate. The positive effect of Y manifests more obviously after 30 cycles, as shown in Fig. 5b. The sharply increased contact resistance in pure Si electrode indicates its rapid breakdown of conduction network, which usually leads to capacity fading during cycling. These results from impedance analysis are in good agreement with the charge–discharge cycling performance.

Fig. 6 is the SEM and EDX images of pure Si and Si–Y thin films with the thickness of Y thin film of 22.5 nm after 50 cycles. For the SEM testing, the electrodes cycled 50 times were dismantled and washed in dimethyl carbonate to remove residual electrolyte solvent and $LiPF_6$ salt, followed by drying with hair drier before analysis. Because of the volume change during lithium insertion/extraction, the pure Si film in Fig. 6a has pulverized, cracked and lost contact with current collector resulting in the mechanical instability and poor cyclability. In contrast, the surface morphology of the Si–Y electrolyte in Fig. 6c is smoother with the island structure. These islands adhere strongly to substrate and provide electrical connection, which can reduce the stress that arises from volume change during cycling [3]. The SEM observations are in good agreement with the results from impedance analysis and the charge–discharge cycling performance. The EDX images of the samples in Fig. 6b,d evince the presence of active materials including Si and Si–Y that have no change after cycling. In summary, the Si–Y anode configuration can offer a good conductive and stress-alleviated environment to keep the stability of electrodes and greatly improve the cycle-life of the host materials.

3.3. Diffusion coefficient of Li^+

Cyclic voltammetry is an effective way to determine the diffusion coefficient of Li^+. Fig. 7 shows the cyclic voltammetry curves and the fitting straight-lines. The cyclic voltammetry curves are measured at potential scan rates from 0.10 to 0.25 mV s^{-1}. From low to high scan rate, the rate-determining steps of the electrochemical reaction may change from surface reaction to semi-infinite lithium diffusion in the film [41]. The dependence of the peak current (I_p) on the potential scan rate (ν) can be used to distinguish these different cases [42]. When the peak current is proportional to the potential scan rates, the process of Li^+ insertion/extraction is under

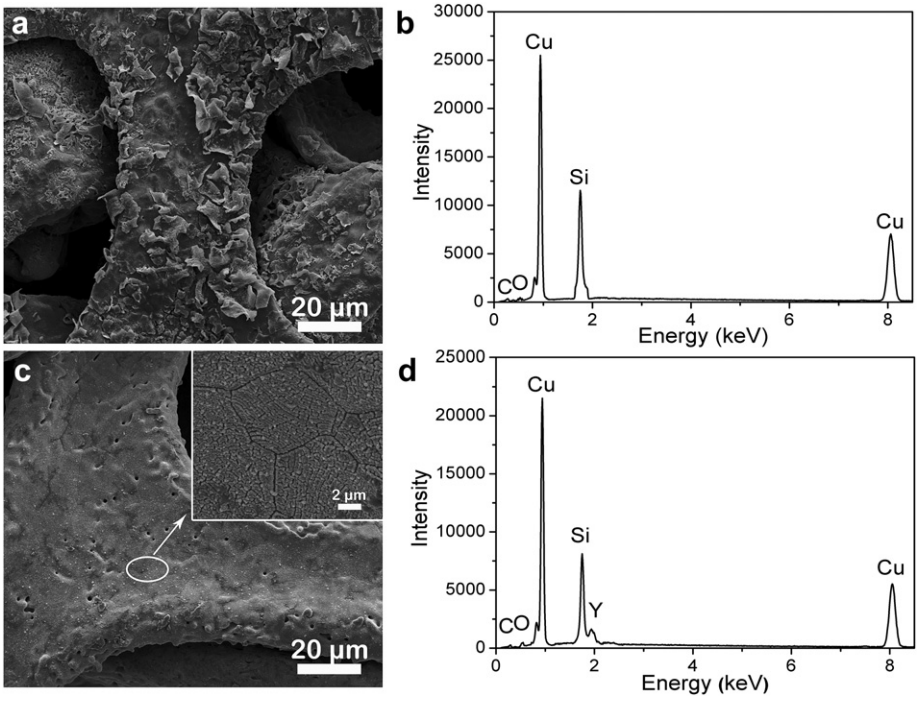

Fig. 6. SEM and EDX images of pure Si thin film (a, b) and Si–Y (c, d) thin film with the thickness of Y thin film of 22.5 nm cycled 50 times.

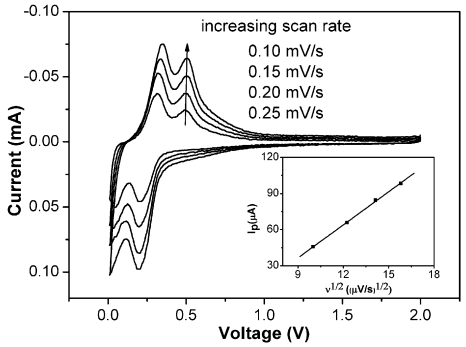

Fig. 7. Cyclic voltammograms at different scan rates for the Si–Y thin film and the dependence of peak current (I_p) on the square of the potential scan rate ($\nu^{1/2}$) for the cathodic peak.

surface reaction control. In the case of semi-infinite diffusion-controlled process, the peak current varies directly with the square root of the potential scan rate ($\nu^{1/2}$), which can be expressed by the classical Randles-Sevchik equation [43]:

$$I_p = 2.69 \times 10^5 n^{3/2} A D_0^{1/2} \nu^{1/2} C_0$$

where n is the number of electrons involved in the electrode reaction (1 for Li^+), A is the contact area of the electrode, D_0 is the diffusion coefficient of Li^+ and C_0 is the bulk concentration of Li^+. We can calculate the apparent diffusion coefficient of Li^+ in the Si thin film with Y as doped layer assuming semi-infinite diffusion. The diffusion coefficients calculated from the slopes of I_p versus $\nu^{1/2}$ for the cathodic peak at ~0.20 V is 2.43×10^{-8} cm^2 s^{-1}, which is larger than that of amorphous Si thin film (2.36×10^{-9} cm^2 s^{-1}) [26]. Therefore, the joining of Y thin film can improve the Li-ion kinetic property at the interface of the Si electrode and the electrolyte.

4. Conclusions

In conclusion, Si–Y multi-layer thin films have been deposited on copper foam layer-by-layer by magnetron sputtering and investigated as anode materials of rechargeable Li-ion batteries. The electrochemical properties depend on the thickness of Y thin films. The thin film with the optimal thickness (22.5 nm) of Y thin film shows excellent electrode stability and cycling performance with a high reversible capacity of 2450 mAh g^{-1} and a Coulombic efficiency above 95% under a current density of 0.4 C after 50 cycles. The diffusion coefficients of Li^+ in the Si–Y thin film are determined to be 2.43×10^{-8} cm^2 s^{-1}. The present results show that the use of Y thin film acts as a buffer layer to suppress the volume variation of the active Si during repeated cycling tests as well as to improve the Li-ion diffusion kinetic property. Therefore, the Si–Y multi-layer thin film is a potential electrode of micro-power Li-ion batteries with high performance.

Acknowledgments

This work was supported by the Research Programs from National 973 (2011CB935900), NSFC (21076108), MOE Innovation Team (IRT0927), and Tianjin High-tech (10JCYBJC08400 and 10SYSYJC27600).

References

[1] S. Bourderau, T. Brousse, D.M. Schleich, Journal of Power Sources 81-82 (1999) 233–236.
[2] G.B. Cho, B.K. Lee, W.C. Sin, K.K. Cho, K.W. Kim, H.J. Ahn, Journal of Alloys and Compounds 449 (2008) 308–312.
[3] T. Moon, C. Kim, B. Park, Journal of Power Sources 155 (2006) 391–394.
[4] F.Y. Cheng, J. Liang, Z.L. Tao, J. Chen, Advanced Materials 23 (2011) 1695–1715.
[5] A. Patil, V. Patil, D.W. Shin, J.W. Choi, D.S. Paik, S.J. Yoon, Materials Research Bulletin 43 (2008) 1913–1942.
[6] J.Y. Xiang, X.L. Wang, X.H. Xia, L. Zhang, Y. Zhou, S.J. Shi, J.P. Tu, Electrochimica Acta 55 (2010) 4921–4925.
[7] L.Z. Zhao, S.J. Hu, Q. Ru, W.S. Li, X.H. Hou, R.H. Zeng, D.S. Lu, Journal of Power Sources 184 (2008) 481–484.
[8] T.D. Hatcharda, J.R. Dahna, Journal of the Electrochemical Society 151 (2004) A1628–A1635.
[9] G. Taillades, N. Benjelloun, J. Sarradin, M. Ribes, Solid State Ionics 152–153 (2002) 119–124.
[10] S.C. Zhang, Z.J. Du, R.X. Lin, T. Jiang, G.R. Liu, X.M. Wu, D.S. Weng, Advanced Materials 22 (2010) 5378–5382.
[11] G.X. Wang, L. Sun, D.H. Bradhurst, S. Zhong, S.X. Dou, H.K. Liu, Journal of Alloys and Compounds 306 (2000) 249–252.
[12] J. Chen, F.Y. Cheng, Accounts of Chemical Research 42 (2009) 713–723.
[13] J. Xie, N. Imanishi, T. Zhang, A. Hirano, Y. Takeda, O. Yamamoto, Materials Chemistry and Physics 120 (2010) 421–425.
[14] B. Peng, F.Y. Cheng, Z.L. Tao, J. Chen, Journal of Chemical Physics 133 (2010) 034701,1–5.
[15] L.B. Hu, H. Wu, S.S. Hong, L.F. Cui, J.R. McDonough, S. Bohy, Y. Cui, Chemical Communications 47 (2011) 367–369.
[16] D. Munao, J.W.M. van Erven, M. Valvo, E. Garcia-Tamayo, E.M. Kelder, Journal of Power Sources 196 (2011) 6695–6702.
[17] B. Peng, J. Chen, Coordination Chemistry Reviews 253 (2009) 2805–2813.
[18] J.P. Rong, C. Masarapu, J. Ni, Z.J. Zhang, B.Q. Wei, ACS Nano 4 (2010) 4683–4690.
[19] M.K. Datta, J. Maranchi, S.J. Chung, R. Epur, K. Kadakia, P. Jampani, P.N. Kumta, Electrochimica Acta 56 (2011) 4717–4723.
[20] Y.N. Zhou, W.J. Li, H.J. Chen, C. Liu, L. Zhang, Z.W. Fu, Electrochemistry Communications 13 (2011) 546–549.
[21] Y. Imai, A. Watanabe, Journal of Alloys and Compounds 509 (2011) 7877–7880.
[22] X.Y. Wang, Z.Y. Wen, Y. Liu, L.Z. Huang, M.F. Wu, Journal of Alloys and Compounds 506 (2010) 317–322.
[23] S.L. Chou, Y. Zhao, J.Z. Wang, Z.X. Chen, H.K. Liu, S.X. Dou, Journal of Physical Chemistry 114 (2010) 15862–15867.
[24] M. Suzukia, J. Suzukia, K. Sekinea, T. Takamura, Journal of Power Sources 146 (2005) 452–456.
[25] Z.Y. Wang, Y. Li, J.Y. Lee, Electrochemistry Communications 11 (2009) 1179–1182.
[26] C.M. Hwang, J.W. Park, Surface & Coatings Technology 205 (2010) S439–S446.
[27] H.J. Pan, J. Zhang, Y.H. Chen, X.D. Zhuo, Y. Yang, Thin Solid Films 519 (2010) 778–783.
[28] C.M. Hwang, J.W. Park, Journal of Power Sources 196 (2011) 6772–6780.
[29] J.B. Kim, B.S. Jun, S.M. Lee, Electrochimica Acta 50 (2005) 3390–3394.
[30] H.X. Li, F.Y. Cheng, Z.Q. Zhu, H.M. Bai, Z.L. Tao, J. Chen, Journal of Alloys and Compounds 509 (2011) 2919–2923.
[31] F.Y. Cheng, J. Shen, B. Peng, Y.D. Pan, Z.L. Tao, J. Chen, Nature Chemistry 3 (2011) 79–84.
[32] J. Chen, L.N. Xu, W.Y. Li, X.L. Gou, Advanced Materials 17 (2005) 582–586.
[33] H. Ma, F.Y. Cheng, J. Chen, J.Z. Zhao, C.S. Li, Z.L. Tao, J. Liang, Advanced Materials 19 (2007) 4067–4070.
[34] L.F. Cui, J. Shen, F.Y. Cheng, Z.L. Tao, J. Chen, Journal of Power Sources 196 (2011) 2195–2201.
[35] V.S. Sudavtsova, N.V. Kotova, Inorganic Chemistry 43 (2007) 567–572.
[36] V.A. Sethuraman, K. Kowolik, V. Srinivasan, Journal of Power Sources 196 (2011) 393–398.
[37] W. Wang, M.K. Datta, P.N. Kumta, Journal of Materials Chemistry 17 (2007) 3229–3237.
[38] S. Yoon, I. Hwang, C.W. Lee, H.S. Ko, K.H. Han, Journal of Electroanalytical Chemistry 655 (2011) 32–38.
[39] T. Jiang, S.C. Zhang, X.P. Qiu, W.T. Zhu, L.Q. Chen, Electrochemistry Communications 9 (2007) 930–934.
[40] Y.C. Chang, H.J. Sohn, Journal of the Electrochemical Society 147 (2000) 50–58.
[41] L.B. Chen, J.Y. Xie, H.C. Yu, T.H. Wang, Journal of Applied Electrochemistry 39 (2009) 1157–1162.
[42] N. Ding, J. Xu, Y.X. Yao, G. Wegner, X. Fang, C.H. Chen, I. Lieberwirth, Solid State Ionics 180 (2009) 222–225.
[43] A.J. Bard, L.R. Faulkner, Electrochemical Methods: Fundamentals and Applications, second ed. Wiley, New York, 2001, pp. 231.